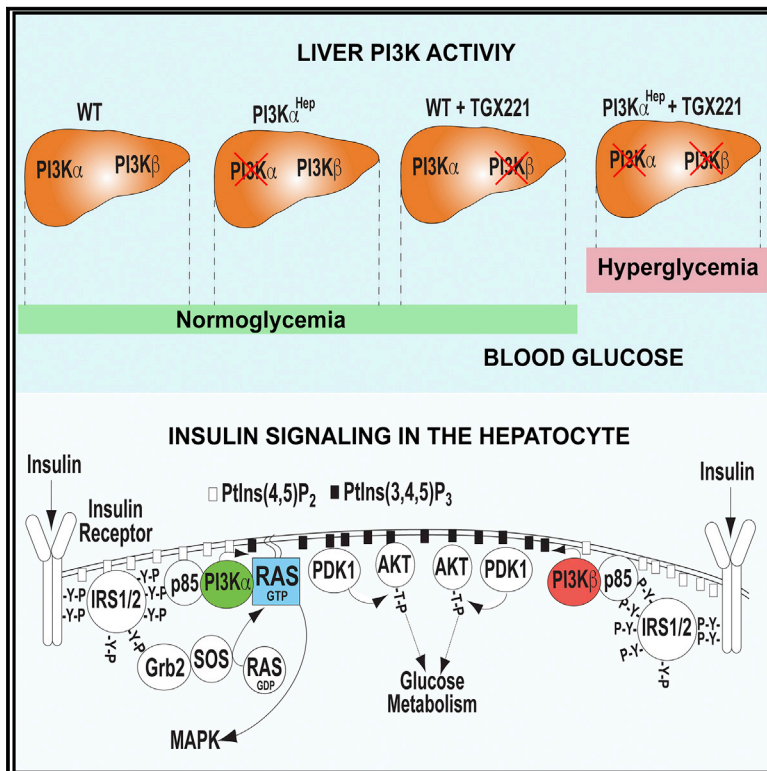


# Cell Metabolism

## Insulin-Driven PI3K-AKT Signaling in the Hepatocyte Is Mediated by Redundant PI3K $\alpha$ and PI3K $\beta$ Activities and Is Promoted by RAS

### Graphical Abstract



### Authors

Angela Molinaro, Barbara Becattini, Arianna Mazzoli, ..., Antonio Molinaro, Fredrik Bäckhed, Giovanni Solinas

### Correspondence

giovanni.solinas@wlab.gu.se

### In Brief

Insulin signaling is believed to be mediated by PI3K $\alpha$  activity, which depends on RAS. Molinaro et al. show that maximal insulin-induced AKT phosphorylation, but not downstream signaling, depends on RAS. They show that insulin signaling in hepatocytes and insulin action on glycemia are mediated by redundant PI3K $\alpha$  and PI3K $\beta$  activities.

### Highlights

- Insulin-driven AKT phosphorylation, but not downstream signaling, is promoted by RAS
- RAS action on AKT phosphorylation depends on PI3K $\alpha$
- Insulin signaling in hepatocytes is driven by redundant PI3K $\alpha$  and PI3K $\beta$  activities
- Compound and not single-isoform inhibition of PI3K $\alpha$  and PI3K $\beta$  causes hyperglycemia

# Insulin-Driven PI3K-AKT Signaling in the Hepatocyte Is Mediated by Redundant PI3K $\alpha$ and PI3K $\beta$ Activities and Is Promoted by RAS

Angela Molinaro,<sup>1,6</sup> Barbara Becattini,<sup>1,6</sup> Arianna Mazzoli,<sup>1</sup> Augusto Bleve,<sup>1,4</sup> Lucia Radici,<sup>1</sup> Ingela Maxvall,<sup>2</sup> Victoria Rotter Sopasakis,<sup>1,5</sup> Antonio Molinaro,<sup>1</sup> Fredrik Bäckhed,<sup>1,3</sup> and Giovanni Solinas<sup>1,7,\*</sup>

<sup>1</sup>The Wallenberg Laboratory and Sahlgrenska Center for Cardiovascular and Metabolic Research, Department of Molecular and Clinical Medicine, Institute of Medicine, University of Gothenburg, Gothenburg, Sweden

<sup>2</sup>Translational Science, Cardiovascular, Renal and Metabolism, IMED Biotech Unit, AstraZeneca, Gothenburg, Sweden

<sup>3</sup>Novo Nordisk Foundation Center for Basic Metabolic Research, Section for Metabolic Receptology and Enteroendocrinology, Faculty of Health Sciences, University of Copenhagen, 2200 Copenhagen, Denmark

<sup>4</sup>Present address: Humanitas Clinical and Research Center, Milan, Italy

<sup>5</sup>Present address: Department of Clinical Chemistry and Transfusion Medicine, Institute of Biomedicine, University of Gothenburg, Gothenburg, Sweden

<sup>6</sup>These authors contributed equally

<sup>7</sup>Lead Contact

\*Correspondence: [giovanni.solinas@wlab.gu.se](mailto:giovanni.solinas@wlab.gu.se)

<https://doi.org/10.1016/j.cmet.2019.03.010>

## SUMMARY

Phosphatidylinositol-3-kinase (PI3K) activity is aberrant in tumors, and PI3K inhibitors are investigated as cancer therapeutics. PI3K signaling mediates insulin action in metabolism, but the role of PI3K isoforms in insulin signaling remains unresolved. Defining the role of PI3K isoforms in insulin signaling is necessary for a mechanistic understanding of insulin action and to develop PI3K inhibitors with optimal therapeutic index. We show that insulin-driven PI3K-AKT signaling depends on redundant PI3K $\alpha$  and PI3K $\beta$  activities, whereas PI3K $\delta$  and PI3K $\gamma$  are largely dispensable. We have also found that RAS activity promotes AKT phosphorylation in insulin-stimulated hepatocytes and that promotion of insulin-driven AKT phosphorylation by RAS depends on PI3K $\alpha$ . These findings reveal the detailed mechanism by which insulin activates AKT, providing an improved mechanistic understanding of insulin signaling. This improved model for insulin signaling predicts that isoform-selective PI3K inhibitors discriminating between PI3K $\alpha$  and PI3K $\beta$  should

be dosed below their hyperglycemic threshold to achieve isoform selectivity.

## INTRODUCTION

The class-1 phosphatidylinositide 3-kinases (PI3K)-AKT pathway links the activation of the insulin receptor to glucose metabolism (Boucher et al., 2014; Czech, 2017; Haeusler et al., 2018; Titchenell et al., 2017; White, 2014). Insulin also induces the RAS mitogen activated protein kinase (MAPK) pathway, which has not been implicated in the metabolic action of insulin (Boucher et al., 2014; Czech, 2017; Haeusler et al., 2018; Titchenell et al., 2017; White, 2014). PI3K signaling is frequently altered in cancer and is intensively investigated as target for cancer therapy (Fruman et al., 2017; Goncalves et al., 2018; Janku et al., 2018). However, pan-PI3K inhibitors have shown limited efficacy in cancer monotherapies (Fruman et al., 2017; Goncalves et al., 2018; Janku et al., 2018). This was proposed to be due to the effects of PI3K inhibitors on insulin signaling, leading to hyperglycemia and hyperinsulinemia, which dampens their therapeutic index (Hopkins et al., 2018).

As there are four different PI3Ks (PI3K $\alpha$ , PI3K $\beta$ , PI3K $\delta$ , and PI3K $\gamma$ ) (Burke and Williams, 2015), isoform-selective PI3K

## Context and Significance

Many tumors depend on the activity of the phosphatidylinositol-3-kinases (PI3Ks) protein to grow. However, as this protein is involved in insulin action, blocking it in the clinic can cause high blood sugar, thus limiting its therapeutic efficacy against cancer. Since there are four PI3Ks (PI3K $\alpha$ , PI3K $\beta$ , PI3K $\delta$ , and PI3K $\gamma$ ), targeting specific isoforms may separate the beneficial effects of blocking PI3K for cancer treatment from the harmful effects on insulin action. Molinaro et al. investigated the mechanisms of PI3K activation by insulin and found that high blood sugar develops only when PI3K $\alpha$  and PI3K $\beta$  are both inhibited. This finding helps us understanding better how insulin works and indicates that inhibitors recognizing between PI3K $\alpha$  and PI3K $\beta$  may be effective in cancer therapies.

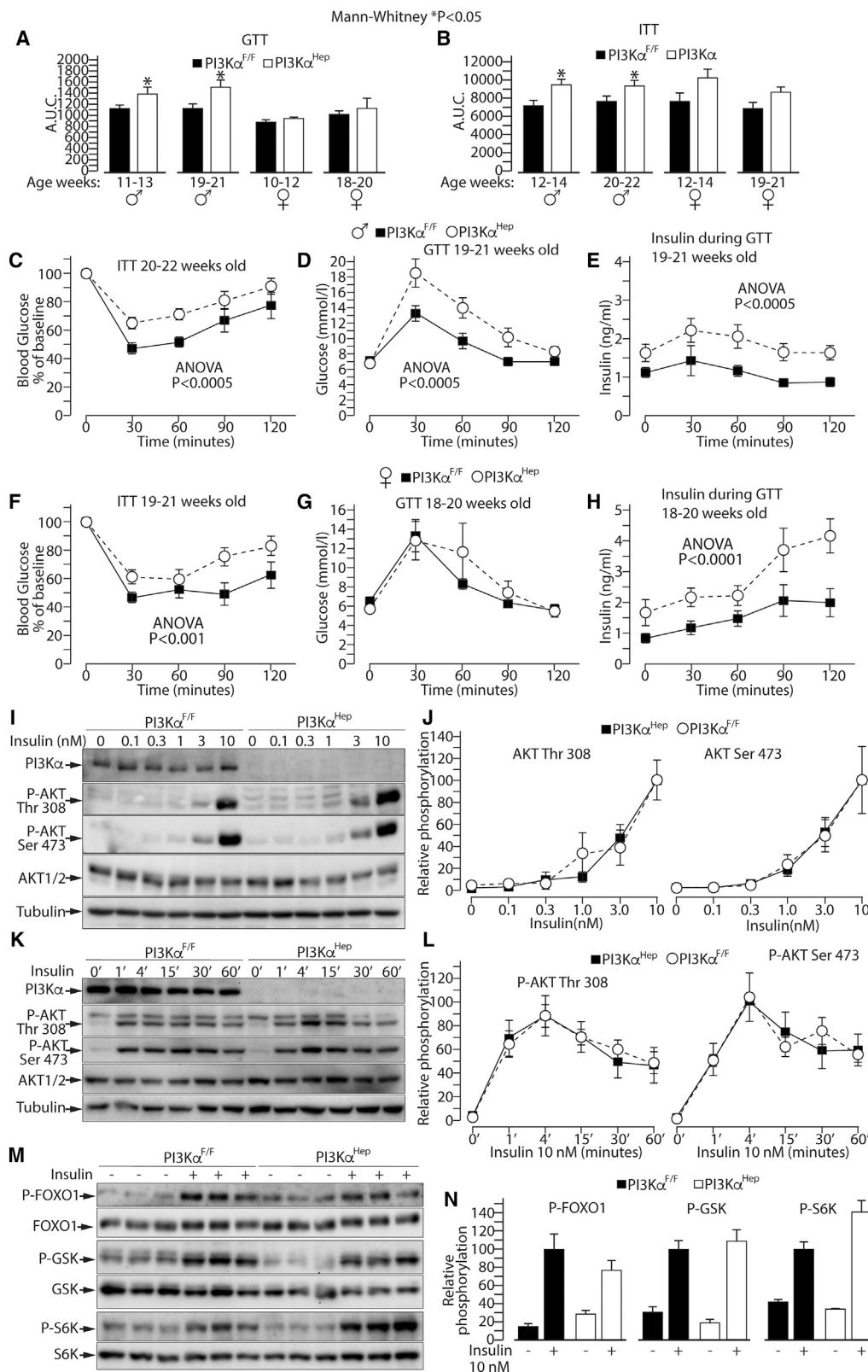


**Figure 1. Loss of PI3K $\alpha$  in the Hepatocyte Is Largely Compensated by a Redundant PI3K Activity**

(A and B) Areas under the curve of glucose tolerance tests (GTT) (A) and of insulin tolerance tests (ITT) (B) of PI3K $\alpha^{F/F}$  and PI3K $\alpha^{Hep}$  male and female mice at the indicated age.

(legend continued on next page)

inhibitors, which do not interfere with the metabolic action of insulin, may prove effective in cancer therapies. However, the role of specific PI3Ks isoforms in insulin action remains unresolved (Boucher et al., 2014; Czech, 2017; Haeusler et al., 2018; Titchenell et al., 2017; White, 2014).

Different studies investigated the role of specific PI3K isoforms in insulin signaling: in cell lines using isoform-specific PI3K inhibitors (Knight et al., 2006) or *in vivo* using genetically modified mice (Chattopadhyay et al., 2011; Ciraolo et al., 2008; Foukas et al., 2006; Jia et al., 2008; Sopasakis et al., 2010), and they came to the conclusion that most of the PI3K activity induced by insulin is mediated by PI3K $\alpha$ . However, the concept that the PI3K activity induced by insulin is mediated by PI3K $\alpha$  is inconsistent with the current model for insulin signaling, where PI3K is activated by direct binding of PI3K regulatory subunits to tyrosine-phosphorylated residues in a RAS-independent manner (Boucher et al., 2014; Czech, 2017; Haeusler et al., 2018; Titchenell et al., 2017; White, 2014). Indeed, structural and functional studies indicate that in the absence of an active RAS GTPase, PI3K $\alpha$  activation is compromised, as PI3K $\alpha$  needs to form a complex with an active RAS to functionally interact with the plasma membrane (Buckles et al., 2017; Siempelkamp et al., 2017; Vadas et al., 2011). Furthermore, it was reported that patients with *PIK3CA*-related overgrowth syndrome (PROS) receiving a low dosage of the PI3K $\alpha$ -selective inhibitor BYL719 displayed a dramatic improvement of their condition, with most subjects showing no effects on glycemia (Venot et al., 2018). This observation cannot be easily explained by a model where insulin action in glucose metabolism is mostly mediated by PI3K $\alpha$ .

To better understand insulin signaling, we investigated the role of PI3K $\alpha$  and RAS in insulin-driven AKT signaling within the hepatocyte, the major cell target for insulin action on glucose production (Edgerton et al., 2017; Michael et al., 2000).

## RESULTS

### Loss of PI3K $\alpha$ in the Hepatocyte Is Largely Compensated by Another PI3K

Two different laboratories independently generated mice lacking PI3K $\alpha$  selectively in their hepatocytes (PI3K $\alpha$ <sup>Hep</sup>) to investigate the role of PI3K $\alpha$  in insulin signaling and glucose homeostasis (Chattopadhyay et al., 2011; Sopasakis et al., 2010). These studies consistently indicate a role for hepatic PI3K $\alpha$  in glucose homeostasis, but they also show relevant differences on the quantitative contribution of PI3K $\alpha$  to insulin action. We hypothe-

sized that this difference is consequent to the fact that in the first study, PI3K $\alpha$ <sup>Hep</sup> mice gained more weight than LoxP floxed control mice (PI3K $\alpha$ <sup>F/F</sup>). Hence, we phenotyped weight-matched littermate PI3K $\alpha$ <sup>Hep</sup> mice and PI3K $\alpha$ <sup>F/F</sup> mice from the first study (Figures S1A–S1D) (Sopasakis et al., 2010). PI3K $\alpha$ <sup>Hep</sup> mice did not develop hyperglycemia but only some insulin intolerance, which was largely compensated by a mild hyperinsulinemia, as a moderate glucose intolerance was observed only in male mice (Figures 1A–1H and S1E–S1H). Hence, ablation of PI3K $\alpha$  in hepatocytes does not cause hyperglycemia, nor does it reproduce the severe metabolic phenotype of mice lacking the insulin receptor in their hepatocytes (Michael et al., 2000), mice expressing a dominant negative PI3K adaptor subunit in their livers (Miyake et al., 2002), or mice lacking hepatic AKT1 and AKT2 (Titchenell et al., 2016; Wang et al., 2016).

To clarify the role of PI3K $\alpha$  in insulin signaling, we investigated insulin-induced AKT phosphorylation in primary hepatocytes from PI3K $\alpha$ <sup>Hep</sup> mice and littermate PI3K $\alpha$ <sup>F/F</sup> mice. Loss of PI3K $\alpha$  did not lead to a significant reduction of insulin-driven AKT signaling in hepatocytes (Figures 1I–1N), revealing that loss of PI3K $\alpha$  is largely compensated by another PI3K. Somatic ablation of PI3K $\alpha$  in hepatocytes from PI3K $\alpha$ <sup>F/F</sup> mice by adenoviral delivery of Cre recombinase confirmed that insulin drives AKT phosphorylation in hepatocytes lacking PI3K $\alpha$  (Figures S1I–S1K), indicating that preserved insulin signaling in hepatocytes from PI3K $\alpha$ <sup>Hep</sup> mice is not due to developmental compensations. Furthermore, hepatocytes from PI3K $\alpha$ <sup>F/F</sup> mice and from PI3K $\alpha$ <sup>Hep</sup> mice displayed similar levels of other PI3K catalytic and regulatory subunits or insulin receptor substrates (IRSs) 1 and 2 (Figures S2A and S2B).

Overall, our results indicate that PI3K $\alpha$  action in insulin signaling in the hepatocyte is functionally redundant with another PI3K.

### Insulin-Dependent AKT Signaling in the Hepatocyte Is Mediated by Redundant PI3K $\alpha$ and PI3K $\beta$ Activities

To identify the PI3K isoform compensating for PI3K $\alpha$  ablation, we measured the inhibition curves of insulin-induced AKT phosphorylation in hepatocytes from PI3K $\alpha$ <sup>Hep</sup> mice and littermate PI3K $\alpha$ <sup>F/F</sup> mice exposed to different doses of a panel of isoform-selective PI3K inhibitors (Table S1).

Insulin-induced AKT phosphorylation was reduced in a similar manner by PI3K $\alpha$  specific inhibitors in PI3K $\alpha$ <sup>Hep</sup> hepatocytes and PI3K $\alpha$ <sup>F/F</sup> hepatocytes, and complete inhibition was observed only at the highest concentrations, where these compounds are not selective for PI3K $\alpha$  (Figures 2A–2D and Table S1).

(C–E) ITT (C), GTT (D), and insulin levels (E) during GTT of PI3K $\alpha$ <sup>F/F</sup> and PI3K $\alpha$ <sup>Hep</sup> male mice at the indicated age.

(F–H) ITT (F), GTT (G), and insulin levels (H) during GTT of PI3K $\alpha$ <sup>F/F</sup> and PI3K $\alpha$ <sup>Hep</sup> female mice at the indicated age.

(I) Immunoblot analysis of insulin-driven AKT phosphorylation in primary hepatocytes from PI3K $\alpha$ <sup>F/F</sup> and PI3K $\alpha$ <sup>Hep</sup> mice stimulated for 8 min with increasing doses of insulin as indicated.

(J) Quantification of the blots in (I).

(K) Immunoblot analysis of insulin-driven AKT phosphorylation in primary hepatocytes from PI3K $\alpha$ <sup>F/F</sup> and PI3K $\alpha$ <sup>Hep</sup> mice stimulated with 10 nM insulin for the indicated time-points.

(L) Quantification of the blots in (K).

(M) Immunoblot analysis of insulin-driven phosphorylation of FOXO1, GSK, and S6K in hepatocytes from PI3K $\alpha$ <sup>F/F</sup> and PI3K $\alpha$ <sup>Hep</sup> mice stimulated with 10 nM insulin for 8 min.

(N) Quantification of the blots in (M).

(A–H), n = 8–12 male mice and n = 7–9 female mice; (I and J), n = 5 mice per genotype; (K–N), n = 3 mice per genotype.

Data are represented as mean  $\pm$  SEM. P values: (A) and (B), Mann-Whitney; (C–H), two-way ANOVA.

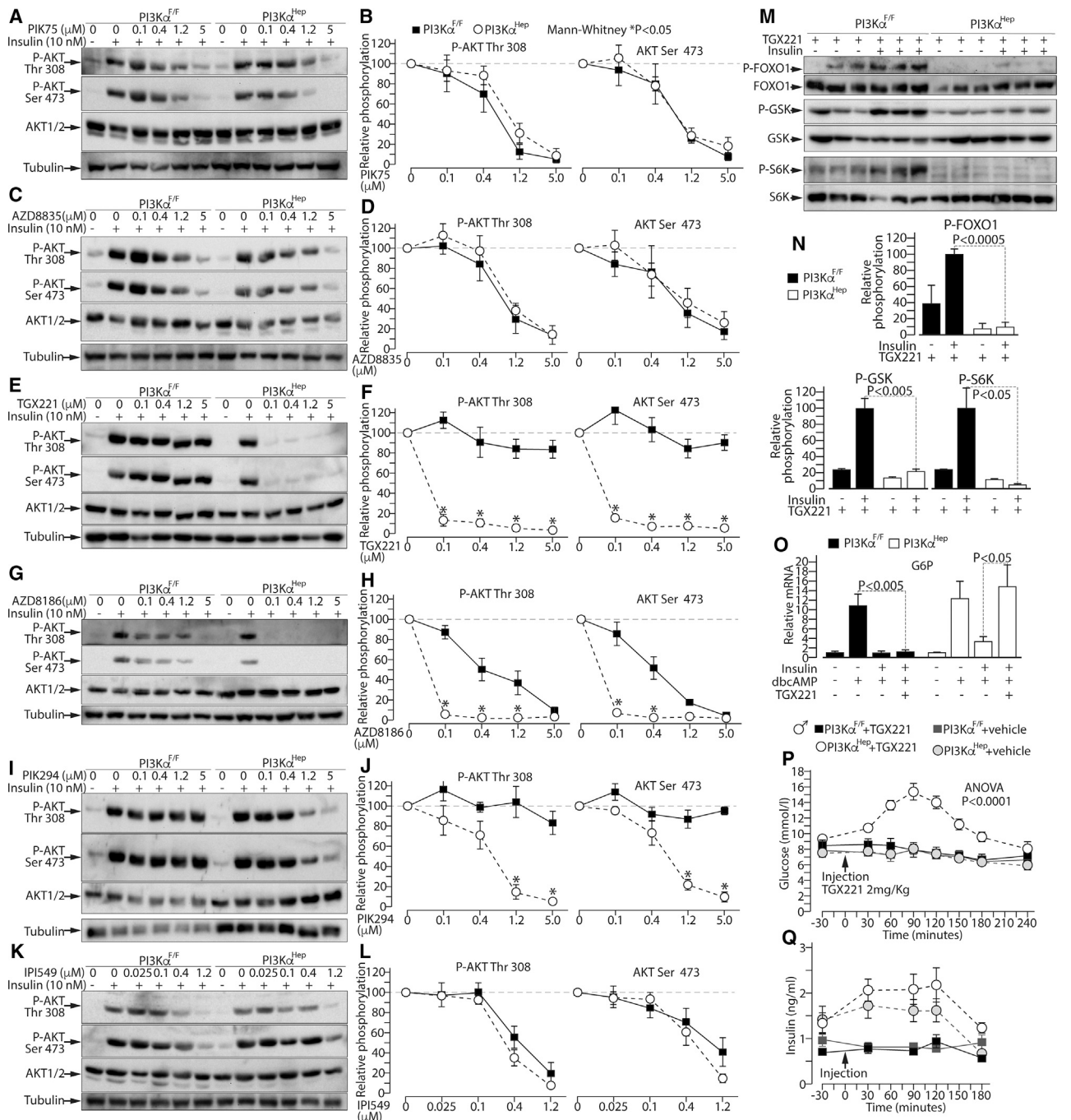


**Figure 2. Insulin-Driven AKT Signaling in the Hepatocyte Is Mediated by PI3K $\alpha$ - and PI3K $\beta$ -Redundant Activities**

(A) Immunoblot analysis of insulin-driven AKT phosphorylation in primary mouse hepatocytes from PI3K $\alpha^{F/F}$  and PI3K $\alpha^{Hep}$  mice stimulated for 8 min with 10 nM insulin and exposed to increasing doses of the PI3K $\alpha$ -selective inhibitor PIK75. (B) Inhibition curves of AKT phosphorylation measured in (A). (C and D) Inhibition curves of insulin-driven AKT phosphorylation as for (A) and (B) but using the PI3K $\alpha$ -selective inhibitor AZD8835. (E and F) Inhibition curves of insulin-driven AKT phosphorylation as for (A) and (B) but using the PI3K $\beta$ -selective inhibitor TGX221. (G and H) Inhibition curves of insulin-driven AKT phosphorylation as for (A) and (B) but using the PI3K $\beta$ -selective inhibitor AZD8186. (I and J) Inhibition curves of insulin-driven AKT phosphorylation as for (A) and (B) but using the PI3K $\delta$ -selective inhibitor PIK294. (K and L) Inhibition curves of insulin-driven AKT phosphorylation as for (A) and (B) but using the PI3K $\gamma$ -selective inhibitor IPI549. (M) Immunoblot analysis of insulin-driven phosphorylation of FOXO1, GSK, and S6K in hepatocytes from PI3K $\alpha^{F/F}$  and PI3K $\alpha^{Hep}$  mice stimulated with 10 nM insulin for 8 min in presence of 1  $\mu$ M TGX221. (N) Quantification of the blots in (M).

(legend continued on next page)

Thus, PI3K $\alpha$  action in hepatocyte insulin signaling is redundant with the activity from another PI3K.

Insulin-induced AKT phosphorylation was blunted by the lowest-used dose of PI3K $\beta$ -selective inhibitors (TGX221 and AZD8186) in hepatocytes from PI3K $\alpha$ <sup>Hep</sup> mice but not in hepatocytes from PI3K $\alpha$ <sup>F/F</sup> mice (Figures 2E–2H). The PI3K $\beta$ -selective inhibitor TGX221, which does not inhibit PI3K $\alpha$  at the used doses (Table S1), had no effect on insulin-induced AKT phosphorylation in hepatocytes from PI3K $\alpha$ <sup>F/F</sup> mice, whereas a progressive inhibition was observed in these cells by the PI3K $\beta$  selective inhibitor AZD8186 (Figures 2E–2H), which has a lower IC<sub>50</sub> for PI3K $\alpha$  (Table S1). Time-course analysis of insulin-induced AKT phosphorylation shows that TGX221 blunted insulin signaling specifically in hepatocytes from PI3K $\alpha$ <sup>Hep</sup> mice (Figures S2C–S2F). Hence, hepatocyte insulin signaling depends on PI3K $\alpha$ – and PI3K $\beta$ -redundant kinase activities.

The PI3K $\delta$  selective inhibitor PIK294 blunted insulin-induced AKT phosphorylation specifically in hepatocytes from PI3K $\alpha$ <sup>Hep</sup> mice but only at concentrations that were above its IC<sub>50</sub> for PI3K $\beta$  (Figures 2I and 2J and Table S1). The PI3K $\gamma$  selective inhibitor IPI549 blunted insulin-induced AKT phosphorylation with similar efficacy in hepatocytes from PI3K $\alpha$ <sup>Hep</sup> mice or PI3K $\alpha$ <sup>F/F</sup> mice but only at doses that were above its IC<sub>50</sub> for PI3K $\alpha$  and PI3K $\beta$  (Figures 2K and 2L and Table S1).

Collectively, these results indicate that insulin-induced AKT phosphorylation in the hepatocyte is mediated by redundant PI3K $\alpha$  and PI3K $\beta$  kinase activities, whereas PI3K $\delta$  and PI3K $\gamma$  are largely dispensable.

### PI3K $\beta$ Overexpression and PI3K $\beta$ Silencing Support PI3K $\alpha$ and PI3K $\beta$ Redundancy in Insulin Signaling

The data above contrast with a previous observation showing that mice injected with an adenovirus expressing PI3K $\beta$  display reduced insulin-induced AKT phosphorylation in their livers (Sopasakis et al., 2010). However, this negative effect of PI3K $\beta$  on insulin signaling could be secondary to an *in vivo* toxicity of the adenovirus expressing PI3K $\beta$ . We now show that adenovirus-driven overexpression of PI3K $\beta$  in cultured hepatocytes does not interfere with insulin-induced AKT phosphorylation but leads to constitutive AKT phosphorylation (Figures S2G and S2H). Furthermore, reduction of PI3K $\beta$  protein levels by siRNA decreased insulin-induced AKT phosphorylation in primary hepatocytes from PI3K $\alpha$ <sup>Hep</sup> mice (Figures S2I–S2K).

These results are consistent with the idea that insulin-driven PI3K-AKT signaling in the hepatocyte is driven by redundant PI3K $\alpha$  and PI3K $\beta$  activities.

### Insulin Action on Glycemia Depends on Redundant PI3K $\alpha$ and PI3K $\beta$ Activities

We tested the effects of the PI3K $\beta$  inhibitor TGX221 on metabolic-relevant targets downstream AKT in hepatocytes from PI3K $\alpha$ <sup>F/F</sup> mice and from PI3K $\alpha$ <sup>Hep</sup> mice. Insulin-induced phosphorylation of the transcription factor FOXO1, glycogen syn-

these kinase (GSK), and the ribosomal S6 kinase (S6K) was blunted specifically in hepatocytes lacking PI3K $\alpha$  exposed to TGX221 (Figures 1M, 1N, 2M, and 2N). Furthermore, TGX221 blocked insulin-mediated suppression of the expression of the FOXO1-target gene glucose 6 phosphatase (G6P) in hepatocytes from PI3K $\alpha$ <sup>Hep</sup> mice but not from PI3K $\alpha$ <sup>F/F</sup> mice (Figure 2O). Hence, functional insulin signaling downstream AKT in the hepatocyte is completely blunted by compound inhibition of PI3K $\alpha$  and PI3K $\beta$ .

To test the *in vivo* relevance of this observation, we injected PI3K $\alpha$ <sup>F/F</sup> and PI3K $\alpha$ <sup>Hep</sup> mice with either a low dose of TGX221 (2 mg/Kg) or vehicle. TGX221 had no effects on blood glucose or insulin of PI3K $\alpha$ <sup>F/F</sup> mice (Figures 2P and 2Q) but triggered a marked hyperglycemia in PI3K $\alpha$ <sup>Hep</sup> mice (Figure 2P). Peripheral insulin levels were only marginally elevated by TGX221 compared to those in PI3K $\alpha$ <sup>Hep</sup> mice receiving vehicle only (Figure 2Q). Hence, compound inhibition of PI3K $\alpha$  and PI3K $\beta$  activities blunts functional insulin-driven PI3K-AKT signaling in the hepatocyte and causes hyperglycemia.

### Maximal Insulin-Driven AKT Phosphorylation in the Hepatocyte Depends on RAS

In absence of an input from an active RAS, insulin-induced PI3K $\alpha$  activity should be reduced because of defective interaction of PI3K $\alpha$  with the plasma membrane (Buckles et al., 2017; Siempelkamp et al., 2017; Vadas et al., 2011). PI3K $\alpha$  in a partially activated state should compete with PI3K $\beta$ , whose activity is RAS independent (Fritsch et al., 2013; Siempelkamp et al., 2017), for binding to tyrosine-phosphorylated residues reducing insulin-driven AKT phosphorylation.

Hence, we have investigated insulin signaling in hepatocytes infected with either an adenovirus carrying the RAS dominant negative mutant H-RAS17N or a control virus carrying the green fluorescent protein (GFP). 50 MOIs was the minimal dose of virus necessary to transduce most hepatocytes (Figures S3A and S3C). Compared to WT hepatocytes infected with the control virus, insulin-stimulated hepatocytes infected with 50 MOIs of the H-RAS17N virus showed a dramatic reduction of ERK phosphorylation and no effects on AKT phosphorylation or insulin receptor phosphorylation (Figures 3A and 3D–3G). However, 100 MOIs of H-RAS17N significantly reduced AKT phosphorylation without affecting insulin receptor tyrosine phosphorylation, and a similar result was observed using 200 MOIs of H-RAS17N adenovirus (Figures 3B–3G). Hepatocytes infected with 100 MOIs of H-RAS17N virus did not show signs of toxicity, but 200 MOIs of H-RAS17N virus significantly increased the number of apoptotic hepatocytes (Figures S3B and S3D). H-RAS17N protein levels in cells receiving 50 MOIs, 100 MOIs, or 200 MOIs of adenovirus were respectively about 10 times, 30 times, and 40 times the levels of endogenous H-RAS (Figure S3E).

The higher sensitivity to the effects of H-RAS17N observed for insulin-induced ERK phosphorylation compared to AKT phosphorylation is the logical consequence of the different

(O) qPCR analysis of mRNA levels of glucose 6 phosphatase (G6P) in hepatocytes from PI3K $\alpha$ <sup>F/F</sup> and PI3K $\alpha$ <sup>Hep</sup> mice exposed for 6 h to 100  $\mu$ M dbcAMP in presence or not of either 10 nM insulin or 10 nM insulin with 1  $\mu$ M TGX221.

(P and Q) Blood glucose levels (P) and serum insulin levels (Q) of fed PI3K $\alpha$ <sup>F/F</sup> and PI3K $\alpha$ <sup>Hep</sup> mice receiving one injection of 2 mg/Kg of TGX221 or of vehicle. (A–L), n = 4 mice per genotype; (M–N), n = 3 mice per genotype; (O), n = 7 mice per genotype; (P), n = 6 mice per genotype; (Q), n = 5 mice per genotype. Data are represented as mean  $\pm$  SEM. P values: (B–L) and (O), Mann-Whitney; (N), two-tailed t test; (P) two-way ANOVA.

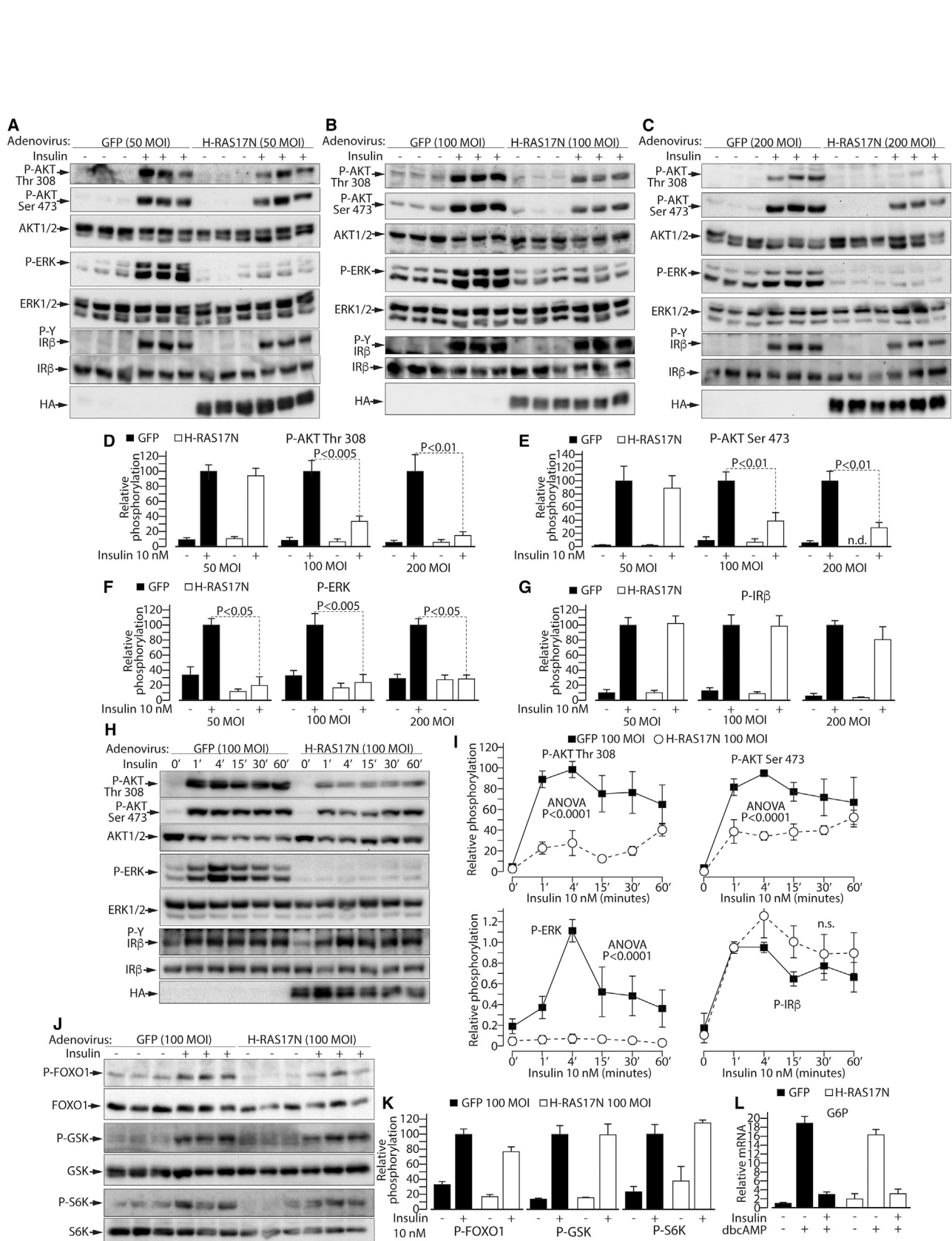


**Figure 3. Insulin-Driven AKT Phosphorylation in Mouse Hepatocytes Is Partially RAS Dependent**

(A) Immunoblot analysis of insulin-induced AKT, ERK, and insulin receptor phosphorylation in primary hepatocytes from WT mice infected with either 50 MOI of a control adenovirus (GFP) or with an adenovirus expressing the RAS dominant negative mutant H-RAS17N.

(B) Immunoblot analysis of insulin signaling as for (A) in mouse hepatocytes infected with 100 MOI of control (GFP) or H-RAS17N adenovirus.

(C) Immunoblot analysis of insulin signaling as for (A) in mouse hepatocytes infected with 200 MOI of control (GFP) or H-RAS17N adenovirus.

(legend continued on next page)

mechanisms of activation of ERK and PI3K $\alpha$  by RAS. RAS-induced ERK phosphorylation was reported to require the formation of active RAS dimers, which occurs only above a minimal density of active RAS at the plasma membrane (Nan et al., 2015; Rajakulendran et al., 2009; Weber et al., 2001), a mechanism particularly sensitive to RAS inhibition (Figures S3F and S3G). By contrast, activation of PI3K $\alpha$  by RAS is believed to be mediated by direct binding of PI3K $\alpha$  to active RAS monomers, promoting a functional interaction of PI3K $\alpha$  with the plasma membrane (Figure S3H) (Buckles et al., 2017; Siempelkamp et al., 2017; Vadas et al., 2011). Since this latter mechanism does not need the formation of RAS dimers, it is expected to require a higher dose of H-RAS17N to be inhibited (Figure S3I).

Time-course analysis of insulin signaling showed that 100 MOIs of H-RAS17N inhibited insulin-induced AKT phosphorylation, but this effect was reduced after one hour of insulin stimulation; ERK phosphorylation was blunted, whereas insulin receptor phosphorylation was not affected (Figures 3H and 3I). However, hepatocytes receiving 100 MOIs of H-RAS17N showed normal insulin-induced phosphorylation of FOXO1, GSK, and S6K as well as insulin-mediated suppression of G6P gene expression (Figures 3J–3L).

Altogether, these results support the idea that RAS promotes insulin-induced AKT phosphorylation, but inhibition of RAS activity in isolation did not impair insulin signaling downstream AKT in mouse hepatocytes.

### The Effects of RAS Blockage on AKT Phosphorylation Depends on PI3K $\alpha$

Infection of primary hepatocytes from WT mice with 200 MOIs of a virus expressing the R-RAS dominant negative mutant R-RAS43N, which does not block the activation of RAS by SOS, did not affect insulin signaling, indicating that the effects of H-RAS17N on AKT phosphorylation depend on the blockage of specific GEFs (Figures S4A and S4B). Furthermore, whereas 100 MOIs of H-RAS17N adenovirus reduced insulin-dependent AKT phosphorylation in hepatocytes from PI3K $\alpha$ <sup>F/F</sup> mice (Figures 4A and 4B), 100 MOIs, or 200 MOIs of H-RAS17N did not reduce AKT phosphorylation in hepatocytes from PI3K $\alpha$ <sup>Hep</sup> mice (Figures 4C, 4D, S4C, and S4D). This observation is consistent with the idea that full activation of PI3K $\alpha$ , but not PI3K $\beta$ , by insulin requires an input from RAS.

### RAS Action in Insulin-Driven AKT Phosphorylation Is Conserved in Human Primary Hepatocytes

To investigate the relevance of the RAS-PI3K $\alpha$  axis to humans, we have performed a dose response for insulin signaling in pri-

mary hepatocytes from human donors (Table S2) infected with either 100 MOIs of H-RAS17N virus or with control GFP adenovirus. H-RAS17N inhibited ERK phosphorylation and AKT phosphorylation without affecting insulin receptor phosphorylation in human hepatocytes exposed to insulin, indicating that the role of RAS in insulin-induced AKT phosphorylation is conserved in humans (Figures 4E and 4F).

### TGX221 and H-RAS17N Do Not Displace p85 from PI3K $\alpha$ , PI3K $\beta$ , or IRS1

To investigate whether TGX221 or H-RAS17N displace PI3K $\alpha$  or PI3K $\beta$  complexes with p85 and IRS1, we performed immunoprecipitations with antibodies against p85 or IRS1 using protein extracts from mouse hepatocytes stimulated with insulin in presence or not of TGX221, or infected with 100 MOIs of the H-RAS17N adenovirus, or a control (GFP) virus. Complexes from p85 immunoprecipitation were probed with antibodies against PI3K $\alpha$  or PI3K $\beta$ , whereas complexes from IRS1 immunoprecipitation were probed with antibodies against p85. Neither TGX221 nor H-RAS17N affected the interaction between p85 and PI3K $\alpha$  or PI3K $\beta$  or the interaction between p85 and IRS1 (Figures S4E–S4H).

## DISCUSSION

The current model of insulin signaling indicates that insulin induces PI3K activity independently from RAS (Boucher et al., 2014; Czech, 2017; Haeusler et al., 2018; Titchenell et al., 2017; White, 2014), and it is believed that most PI3K activity induced by insulin comes from PI3K $\alpha$  (Chattopadhyay et al., 2011; Ciruolo et al., 2008; Foukas et al., 2006; Jia et al., 2008; Knight et al., 2006; Sopasakis et al., 2010). However, PI3K $\alpha$  depends on RAS to be fully activated (Buckles et al., 2017; Siempelkamp et al., 2017; Vadas et al., 2011). Here we solve this apparent paradox: our results identify the specific PI3Ks mediating insulin signaling in the hepatocyte revealing an unexpected role for PI3K $\beta$  and implicate for the first time the RAS-PI3K $\alpha$  axis in insulin-induced AKT phosphorylation. PI3K $\alpha$ <sup>Hep</sup> mice showed a modest insulin resistance. However, PI3K $\alpha$  ablation did not impair insulin signaling in cultured hepatocytes. Hence, the insulin resistance observed *in vivo* may depend on the interaction of hepatocytes with other cell types or may be due to reduced PI3K signaling on targets other than AKT (Hu et al., 2016). Nevertheless, our data consistently indicate that PI3K $\alpha$  action in insulin-induced AKT signaling in the hepatocyte is redundant with another PI3K, which we have found to be PI3K $\beta$ . Importantly, whereas mice lacking either PI3K $\alpha$  or PI3K $\beta$  in their hepatocytes

(D–G) Quantification of (D) AKT threonine 308 phosphorylation, (E) AKT serine 473 phosphorylation, (F) ERK1,2 phosphorylation, and (G) insulin receptor tyrosine phosphorylation of the immunoblots in (A–C).

(H) Immunoblot analysis of insulin-driven AKT phosphorylation in primary mouse hepatocytes infected with either 100 MOIs of GFP adenovirus or H-RAS17N adenovirus, stimulated with 10 nM insulin at the indicated time-points.

(I) Quantification of the immunoblots in (H).

(J) Immunoblot analysis of insulin-driven phosphorylation of FOXO1, GSK, and S6K in primary mouse hepatocytes infected with either 100 MOIs of GFP adenovirus or H-RAS17N adenovirus, stimulated with 10 nM insulin for 8 min.

(K) Quantification of the immunoblots in (J).

(L) qPCR analysis of mRNA levels of glucose 6 phosphatase (G6P) in primary mouse hepatocytes infected with either 100 MOIs of GFP adenovirus or H-RAS17N adenovirus, exposed for 6 h to 100  $\mu$ M of dbcAMP in presence or not of 10 nM insulin.

(A–G), n = 4 mice for 50 MOI, n = 6–7 mice for 100 MOI, and n = 4–5 for 200 MOI experiments; (H–L), n = 3 mice.

Data are represented as mean  $\pm$  SEM. P values: (D–G), Mann-Whitney; (I), two-way ANOVA.

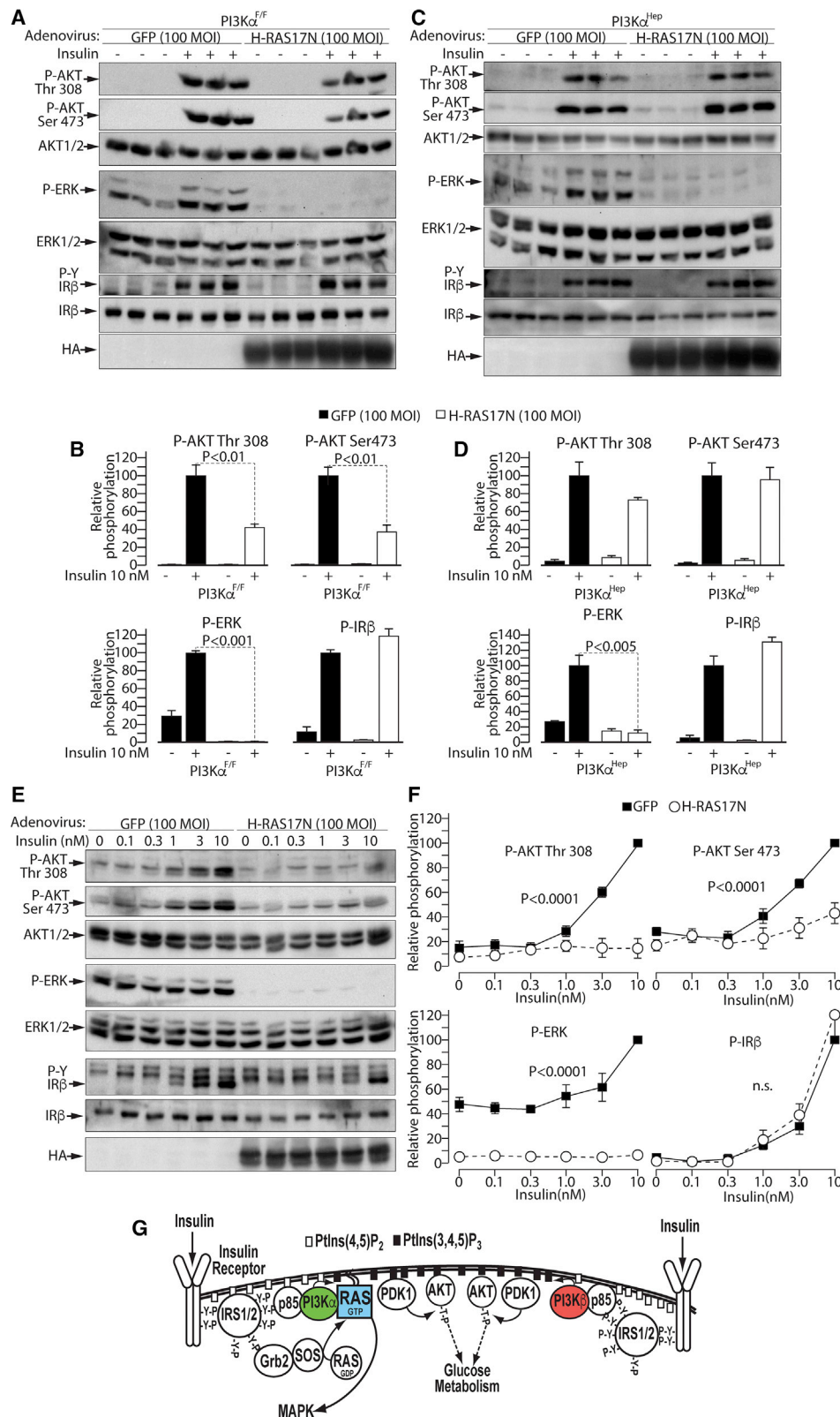


**Figure 4. RAS Action on Insulin-Induced AKT Phosphorylation Depends on PI3K $\alpha$  and Is Conserved in Humans**

(A) Immunoblot analysis of insulin-driven phosphorylation of AKT, ERK, and insulin receptor  $\beta$ -chain in primary hepatocytes from PI3K $\alpha^{F/F}$  mice infected with 100 MOI of either a control GFP adenovirus or an adenovirus expressing the dominant negative mutant H-RAS17N.

(legend continued on next page)

do not show overt hyperglycemia (Chattopadhyay et al., 2011; Jia et al., 2008; Sopasakis et al., 2010), PI3K $\alpha$ <sup>Hep</sup> mice receiving a single injection of a low dose of the PI3K $\beta$  inhibitor TGX221 developed a marked hyperglycemia. Hence, hyperglycemia develops only when PI3K $\alpha$  and PI3K $\beta$  are both inhibited.

Blockage of RAS activity reduced insulin-induced AKT phosphorylation in mouse hepatocytes in a PI3K $\alpha$ -dependent manner but did not affect functional signaling downstream AKT. Hence, residual activity from PI3K $\alpha$  and PI3K $\beta$ , the latter being independent from RAS (Fritsch et al., 2013), is sufficient to drive functional insulin signaling downstream AKT in mouse hepatocytes when RAS activation is blocked.

We thus present an improved, more detailed model for insulin signaling where insulin-induced AKT phosphorylation is driven by the redundant PI3K $\alpha$  and PI3K $\beta$  activities, with RAS sustaining PI3K $\alpha$  activity (Figure 4G). This model has major implications for the study of insulin action and for the development of therapies for the treatment of cancer and PI3K-related overgrowth syndromes. Our model is consistent with data from a recent study showing that a low dose (50 mg/day) of the PI3K $\alpha$  specific inhibitor BYL719 caused a remarkable improvement of the general condition of PROS patients without altering glycemia (Venot et al., 2018). Accordingly, whereas the current model for insulin signaling cannot explain why BYL719 displays a higher hyperglycemic threshold than pan-PI3K inhibitors (Fritsch et al., 2014), our improved model for insulin signaling predicts that BYL719 should cause hyperglycemia only at doses where its specificity for PI3K $\alpha$  is lost. Indeed, the hyperglycemic threshold of BYL719 was measured to be around 20  $\mu$ M, a concentration that is about twenty times higher than the IC<sub>50</sub> of BYL719 for PI3K $\beta$  (Fritsch et al., 2014).

From our model of insulin signaling (Figure 4G), it is deduced that isoform-specific PI3K inhibitors discriminating between PI3K $\alpha$  and PI3K $\beta$  should be used at doses below their hyperglycemic threshold to preserve isoform selectivity.

### Limitations of Study

Our study does not exclude a minor contribution for PI3K $\delta$  in insulin signaling. However, PI3K $\delta$  role in insulin signaling, if any, must be minimal, since compound inhibition of PI3K $\alpha$  and PI3K $\delta$  did not affect insulin signaling.

We have shown that, in young insulin-sensitive mice, hyperglycemia develops only following compound inhibition of PI3K $\alpha$  and PI3K $\beta$  activities. However, our data do not exclude the possibility that inhibition of a single PI3K isoform may cause hyperglycemia in insulin-resistant animals predisposed to hyperglycemia.

Our data from mouse hepatocytes indicate that RAS activity is dispensable for insulin signaling downstream AKT, but our study lacks *in vivo* evidences further supporting this conclusion. Yet,

completely blocking RAS activity *in vivo* in controlled conditions may prove challenging. We observed a more pronounced effect of RAS inhibition on AKT phosphorylation in human hepatocytes. However, this may be consequent to the medical conditions of the donors, and an eventual toxicity of the virus in these cells was not investigated as extensively as for mouse hepatocytes due to limiting material.

### STAR★METHODS

Detailed methods are provided in the online version of this paper and include the following:

- KEY RESOURCES TABLE
- CONTACT FOR REAGENT AND RESOURCE SHARING
- EXPERIMENTAL MODEL AND SUBJECT DETAILS
  - Mice and *In Vivo* Studies
  - Primary Hepatocyte Cell Cultures
  - Production and Precise Titration of Recombinant Adenoviruses
  - Cell Culture Treatments and TUNEL Assay
  - PI3K $\beta$  Silencing in Primary Mouse Hepatocytes
  - qPCR Analysis of Glucose-6-Phosphatase Gene Expression
  - Immunoblot Analysis
  - Immunoprecipitations
  - PI3K Selective Inhibitors
- QUANTIFICATION AND STATISTICAL ANALYSIS

### SUPPLEMENTAL INFORMATION

Supplemental Information can be found online at <https://doi.org/10.1016/j.cmet.2019.03.010>.

### ACKNOWLEDGMENTS

We thank M.C. Magnone and M. Althage at AstraZeneca for their feedback on primary human hepatocytes studies. We thank L. Pirola, who provided the recipient adenovirus, and we are grateful to E. Björnson for his feedback on statistical analysis. This work was supported by funding from the Swiss National Science Foundation (Sinergia grant) 154499, the EFSO Diabetes and Cancer Programme, the Cancerfonden CAN2017/472, the Swedish Research Council 2014-3019, the Novo Nordisk Fonden NNF34410, and by the Diabetes Fonden grants DIA2014-069, DIA2017-232, and DIA2018-384 to G.S.

### AUTHOR CONTRIBUTIONS

G.S. conceived the study, designed the experiments, analyzed data, and wrote the manuscript. Angela Molinaro, B.B., and A. Mazzoli performed experiments and analyzed data. B.B. and Angela Molinaro contributed to editing the manuscript. A.B. and L.R. generated adenovirus vectors. I.M. contributed to human hepatocytes cultures and revised the manuscript. V.R.S. contributed

(B) Quantifications of the immunoblots in (A).

(C) Immunoblot analysis of insulin-driven phosphorylation of AKT, ERK, and insulin receptor  $\beta$ -chain in primary hepatocytes from PI3K $\alpha$ <sup>Hep</sup> mice infected with 100 MOI of either a control GFP adenovirus or an adenovirus expressing the dominant negative mutant H-RAS17N.

(D) Quantifications of the immunoblots in (C). n = 3 mice per genotype.

(E) Immunoblot analysis of insulin-driven AKT phosphorylation, ERK phosphorylation, and insulin receptor tyrosine phosphorylation in human primary hepatocytes infected with either 100 MOI of a GFP-expressing control adenovirus or an adenovirus expressing the dominant negative mutant H-RAS17N.

(F) Quantifications of the AKT, ERK and insulin receptor relative phosphorylation levels from the immunoblots in (E). n = 4 human donors for (E) and (F).

(G) Insulin-driven PI3K-AKT signaling is mediated by PI3K $\alpha$  and PI3K $\beta$  redundant activities and depends on RAS modulation of PI3K $\alpha$  activity.

Data are represented as mean  $\pm$  SEM. P values: (B) and (D), two-tailed t-test; (F), linear regression.

to *in vivo* experiments and data interpretation. Antonio Molinaro and F.B. contributed to mouse hepatocyte culture and revised the manuscript. All authors have read and approved the manuscript.

#### DECLARATION OF INTERESTS

The authors declare no competing interests.

Received: July 12, 2018

Revised: February 4, 2019

Accepted: March 19, 2019

Published: April 11, 2019

#### REFERENCES

- Boucher, J., Kleinridders, A., and Kahn, C.R. (2014). Insulin receptor signaling in normal and insulin-resistant states. *Cold Spring Harb. Perspect. Biol.* *6*, a009191.
- Buckles, T.C., Ziemba, B.P., Masson, G.R., Williams, R.L., and Falke, J.J. (2017). Single-molecule study reveals how receptor and Ras synergistically activate PI3K $\alpha$  and PIP<sub>3</sub> signaling. *Biophys. J.* *113*, 2396–2405.
- Burke, J.E., and Williams, R.L. (2015). Synergy in activating class I PI3Ks. *Trends Biochem. Sci.* *40*, 88–100.
- Chattopadhyay, M., Selinger, E.S., Ballou, L.M., and Lin, R.Z. (2011). Ablation of PI3K p110- $\alpha$  prevents high-fat diet-induced liver steatosis. *Diabetes* *60*, 1483–1492.
- Chaussade, C., Pirola, L., Bonnafous, S., Blondeau, F., Brenz-Verca, S., Tronchère, H., Portis, F., Rusconi, S., Payrastré, B., Laporte, J., and Van Obberghen, E. (2003). Expression of myotubularin by an adenoviral vector demonstrates its function as a phosphatidylinositol 3-phosphate [PtdIns(3)P] phosphatase in muscle cell lines: involvement of PtdIns(3)P in insulin-stimulated glucose transport. *Mol. Endocrinol.* *17*, 2448–2460.
- Ciraolo, E., Iezzi, M., Marone, R., Marengo, S., Curcio, C., Costa, C., Azzolino, O., Gonella, C., Rubinetto, C., Wu, H., et al. (2008). Phosphoinositide 3-kinase p110beta activity: key role in metabolism and mammary gland cancer but not development. *Sci. Signal.* *1*, ra3.
- Czech, M.P. (2017). Insulin action and resistance in obesity and type 2 diabetes. *Nat. Med.* *23*, 804–814.
- Edgerton, D.S., Kraft, G., Smith, M., Farmer, B., Williams, P.E., Coate, K.C., Printz, R.L., O'Brien, R.M., and Cherrington, A.D. (2017). Insulin's direct hepatic effect explains the inhibition of glucose production caused by insulin secretion. *JCI Insight* *2*, e91863.
- Foukas, L.C., Claret, M., Pearce, W., Okkenhaug, K., Meek, S., Peskett, E., Sancho, S., Smith, A.J., Withers, D.J., and Vanhaesebroeck, B. (2006). Critical role for the p110alpha phosphoinositide-3-OH kinase in growth and metabolic regulation. *Nature* *441*, 366–370.
- Fritsch, R., de Krijger, I., Fritsch, K., George, R., Reason, B., Kumar, M.S., Diefenbacher, M., Stamp, G., and Downward, J. (2013). RAS and RHO families of GTPases directly regulate distinct phosphoinositide 3-kinase isoforms. *Cell* *153*, 1050–1063.
- Fritsch, C., Huang, A., Chatenay-Rivauday, C., Schnell, C., Reddy, A., Liu, M., Kauffmann, A., Guthy, D., Erdmann, D., De Pover, A., et al. (2014). Characterization of the novel and specific PI3K $\alpha$  inhibitor NVP-BYL719 and development of the patient stratification strategy for clinical trials. *Mol. Cancer Ther.* *13*, 1117–1129.
- Fruman, D.A., Chiu, H., Hopkins, B.D., Bagrodia, S., Cantley, L.C., and Abraham, R.T. (2017). The PI3K pathway in human disease. *Cell* *170*, 605–635.
- Goncalves, M.D., Hopkins, B.D., and Cantley, L.C. (2018). Phosphatidylinositol 3-kinase, growth disorders, and cancer. *N. Engl. J. Med.* *379*, 2052–2062.
- Haeusler, R.A., McGraw, T.E., and Accili, D. (2018). Biochemical and cellular properties of insulin receptor signalling. *Nat. Rev. Mol. Cell Biol.* *19*, 31–44.
- Hopkins, B.D., Pauli, C., Du, X., Wang, D.G., Li, X., Wu, D., Amadiume, S.C., Goncalves, M.D., Hodakoski, C., Lundquist, M.R., et al. (2018). Suppression of insulin feedback enhances the efficacy of PI3K inhibitors. *Nature* *560*, 499–503.
- Hu, H., Juvekar, A., Lyssiotis, C.A., Lien, E.C., Albeck, J.G., Oh, D., Varma, G., Hung, Y.P., Ullas, S., Luring, J., et al. (2016). Phosphoinositide 3-kinase regulates glycolysis through mobilization of aldolase from the actin cytoskeleton. *Cell* *164*, 433–446.
- Janku, F., Yap, T.A., and Meric-Bernstam, F. (2018). Targeting the PI3K pathway in cancer: are we making headway? *Nat. Rev. Clin. Oncol.* *15*, 273–291.
- Jia, S., Liu, Z., Zhang, S., Liu, P., Zhang, L., Lee, S.H., Zhang, J., Signoretti, S., Loda, M., Roberts, T.M., and Zhao, J.J. (2008). Essential roles of PI(3)K-p110beta in cell growth, metabolism and tumorigenesis. *Nature* *454*, 776–779.
- Knight, Z.A., Gonzalez, B., Feldman, M.E., Zunder, E.R., Goldenberg, D.D., Williams, O., Loewith, R., Stokoe, D., Balla, A., Toth, B., et al. (2006). A pharmacological map of the PI3-K family defines a role for p110alpha in insulin signaling. *Cell* *125*, 733–747.
- Michael, M.D., Kulkarni, R.N., Postic, C., Previs, S.F., Shulman, G.I., Magnuson, M.A., and Kahn, C.R. (2000). Loss of insulin signaling in hepatocytes leads to severe insulin resistance and progressive hepatic dysfunction. *Mol. Cell* *6*, 87–97.
- Miyake, K., Ogawa, W., Matsumoto, M., Nakamura, T., Sakaue, H., and Kasuga, M. (2002). Hyperinsulinemia, glucose intolerance, and dyslipidemia induced by acute inhibition of phosphoinositide 3-kinase signaling in the liver. *J. Clin. Invest.* *110*, 1483–1491.
- Nan, X., Tamgüney, T.M., Collisson, E.A., Lin, L.J., Pitt, C., Galeas, J., Lewis, S., Gray, J.W., McCormick, F., and Chu, S. (2015). Ras-GTP dimers activate the mitogen-activated protein kinase (MAPK) pathway. *Proc. Natl. Acad. Sci. USA* *112*, 7996–8001.
- Rajakulendran, T., Sahmi, M., Lefrançois, M., Sicheri, F., and Therrien, M. (2009). A dimerization-dependent mechanism drives RAF catalytic activation. *Nature* *461*, 542–545.
- Siempelkamp, B.D., Rathinaswamy, M.K., Jenkins, M.L., and Burke, J.E. (2017). Molecular mechanism of activation of class IA phosphoinositide 3-kinases (PI3Ks) by membrane-localized HRas. *J. Biol. Chem.* *292*, 12256–12266.
- Sopasakis, V.R., Liu, P., Suzuki, R., Kondo, T., Winnay, J., Tran, T.T., Asano, T., Smyth, G., Sajan, M.P., Farese, R.V., et al. (2010). Specific roles of the p110alpha isoform of phosphatidylinositol 3-kinase in hepatic insulin signaling and metabolic regulation. *Cell Metab.* *11*, 220–230.
- Titchenell, P.M., Quinn, W.J., Lu, M., Chu, Q., Lu, W., Li, C., Chen, H., Monks, B.R., Chen, J., Rabinowitz, J.D., and Birnbaum, M.J. (2016). Direct hepatocyte insulin signaling is required for lipogenesis but is dispensable for the suppression of glucose production. *Cell Metab.* *23*, 1154–1166.
- Titchenell, P.M., Lazar, M.A., and Birnbaum, M.J. (2017). Unraveling the regulation of hepatic metabolism by insulin. *Trends Endocrinol. Metab.* *28*, 497–505.
- Vadas, O., Burke, J.E., Zhang, X., Berndt, A., and Williams, R.L. (2011). Structural basis for activation and inhibition of class I phosphoinositide 3-kinases. *Sci. Signal.* *4*, re2.
- Venot, Q., Blanc, T., Rabia, S.H., Berteloot, L., Ladraa, S., Duong, J.P., Blanc, E., Johnson, S.C., Huguin, C., Boccara, O., et al. (2018). Targeted therapy in patients with PIK3CA-related overgrowth syndrome. *Nature* *558*, 540–546.
- Wang, Q., Yu, W.N., Chen, X., Peng, X.D., Jeon, S.M., Birnbaum, M.J., Guzman, G., and Hay, N. (2016). Spontaneous hepatocellular carcinoma after the combined deletion of Akt isoforms. *Cancer Cell* *29*, 523–535.
- Weber, C.K., Slupsky, J.R., Kalmes, H.A., and Rapp, U.R. (2001). Active Ras induces heterodimerization of cRaf and BRaf. *Cancer Res.* *61*, 3595–3598.
- White, M.F. (2014). IRS2 integrates insulin/IGF1 signalling with metabolism, neurodegeneration and longevity. *Diabetes Obes. Metab.* *16 (Suppl 1)*, 4–15.

## STAR★METHODS

### KEY RESOURCES TABLE

REAGENT or RESOURCE	SOURCE	IDENTIFIER
<b>Antibodies</b>		
AKT Phospho (Thr308)	Cell Signaling	4056
AKT Phospho (Ser373) XP	Cell Signaling	4060
AKT	Cell Signaling	9272
Erk 1/2 (p44/42 MAPK) Phospho(Thr202/Tyr204) XP	Cell Signaling	9101
Erk 1/2 (p44/42 MAPK)	Cell Signaling	9102
Phospho Tyrosine Clone 4G10	Millipore	05-321
Insulin Receptor $\beta$ -chain	Cell Signaling	3025
FoxO1 Phospho (Ser256)	Cell Signaling	9461
FoxO1	Cell Signaling	2880
GSK Phospho-3Beta (Ser9)	Cell Signaling	9336
GSK	Cell Signaling	9315
IRS1	Millipore	06248
IRS2	Millipore	MAB515
PI3K p85	Cell Signaling	4257
PI3K p85 $\alpha$	Abcam	Ab133595
PI3K p55 $\gamma$	Abcam	Ab238509
p70 S6K Phospho (Thr389)	Cell Signaling	9206
p70 S6K	Cell Signaling	2708
Tubulin $\alpha/\beta$	Cell Signaling	2148
PI3K $\alpha$	Cell Signaling	4249
PI3K $\beta$	Cell Signaling	3011
PI3K $\delta$	Millipore	04-401
PI3K $\gamma$	a gift of Prof. Matthias Wymann University of Basel	(Russian)
Hemagglutinin HA	Sigma	H3663
HRAS	Santa Cruz	Sc53959
<b>Chemicals, Peptides, Recombinant Proteins, and Inhibitors</b>		
Insulin	Humalog Lilly	VL7510
Glucose	Acros	410955000
BSA	Fisher Scientific	BP9702
Guanidinium thiocyanate	Sigma	G6639
Sarkosyl (N-lauroylsarcosine)	Sigma	L5125
Phenol	Acros	221755000
ECL-anti rabbit IgG HRP	GE Healthcare	NA934V
ECL-anti mouse IgG HRP	GE Healthcare	LNA931V
Type I Collagen, from rat tail	Corning	BD #354236
Collagenase, Type IV	Sigma	C5138
N <sup>6</sup> ,2'-O-Dibutyryl adenosine 3',5'-cyclic monophosphate sodium salt	Sigma	D0627
Lipofectamine 3000	ThermoFisher	L3000150
PIK75	Selleckchem	S1205
AZD8835	AstraZeneca	<a href="https://openinnovation.astrazeneca.com/">https://openinnovation.astrazeneca.com/</a>
TGX-221	Selleckchem	S1169
AZD8186	AstraZeneca	<a href="https://openinnovation.astrazeneca.com/">https://openinnovation.astrazeneca.com/</a>

(Continued on next page)

**Continued**

REAGENT or RESOURCE	SOURCE	IDENTIFIER
PIK294	Selleckchem	S2227
IPI549	ChemieTek	CT-IPI549
<b>Critical Commercial Assays</b>		
TUNEL Assay	Roche	12 156 792 910
DNase I	Roche	04 716 728 001
Insulin ELISA Kit	Crystal Chem	Ultra sensitive Mouse ELISA Kit 90080
ImPROM-II Reverse Transcriptase	Promega	A3803
Syber Green (qPCR mix)	Bio Rad	SYBRO Green Supermix 172-5274
Immobilon Western Chemiluminescence HRP substrate	Millipore	WBKLS0500
<b>Oligonucleotides</b>		
	Forward	Reverse
Cyclophilin; GenBank: NM_008907	ATG GTC AAC CCC ACC GTG T	TTT CTG CTG TCT TTG GAA CTT TGT C
G6P; GenBank: NM_032087	CGACTCGCTATCTCCAAGTGA	GTTGAACCACTCTCCGACCA
siRNA scramble (Mouse Negative Control)	Dharmacon	ON-TARGET plus Control Pool D-001810-10-05
siRNA PI3K $\beta$	Dharmacon	ON-TARGET plus SMARTpool L-04088-00-0005
PI3K $\alpha$ <sup>Flox</sup>	CTG TGT AGC CTA GTT TAG AGC AAC CAT CTA	CCT CTC TGA ACA GTT CAT GTT TGA TGG TGA
<b>Experimental Models: Organisms/Strains</b>		
WT	C57BL/6 background	
PI3K $\alpha$ <sup>Flox</sup>	Mixed background	Provided by Victoria Rotter Sopasakis
PI3K $\alpha$ <sup>Hep</sup>	Mixed background	Provided by Victoria Rotter Sopasakis
<b>Plasmids</b>		
PI3K $\beta$	pBacPAK p110 $\beta$ WT Addgene plasmid	55724
H-RAS17N	from UMR cDNA Resource Center, University of Missouri-Rolla	RASH00TN00D0
R-RAS43N	from UMR cDNA Resource Center, University of Missouri-Rolla	RASR00TN00D0
<b>Adenoviruses</b>		
AdVGFP-cre	Coral Vector Core Facility, University of Iowa	VVC-U of Iowa-1174
AdVGFP	Gift from Dr. Luciano Pirola	INSERM 1060 CarMeN Lyon
<b>Software and Algorithms</b>		
Image Lab software (version 5.2.1)	Bio-Rad	<a href="http://www.bio-rad.com/en-us/product/image-lab-software">http://www.bio-rad.com/en-us/product/image-lab-software</a>
Graph Pad Prism 7.0	Graph Pad Software	N/A
AxioVision Software	Imaging Software	Carl Zeiss Microscopy
Bio-Rad CFX Manager	Bio-Rad	N/A
<b>Deposited Data</b>		
<a href="https://doi.org/10.17632/z4388cpmkn.1">https://doi.org/10.17632/z4388cpmkn.1</a>	Immunoblots images	N/A

**CONTACT FOR REAGENT AND RESOURCE SHARING**

Further information and requests for reagents may be directed to the Lead Contact, Giovanni Solinas ([giovanni.solinas@wlab.gu.se](mailto:giovanni.solinas@wlab.gu.se)).

## EXPERIMENTAL MODEL AND SUBJECT DETAILS

### Mice and *In Vivo* Studies

Mice with hepatocyte-specific ablation of PI3K $\alpha$  (PI3K $\alpha^{\text{Hep}}$ ) and control LoxP floxed mice (PI3K $\alpha^{\text{F/F}}$ ) are in 129/SvJ and C57BL/6J mixed background as previously described (Sopasakis et al., 2010) and were provided by Vittoria Rotter Sopasakis. The experimental PI3K $\alpha^{\text{Hep}}$  and PI3K $\alpha^{\text{F/F}}$  control mice were obtained by crossing PI3K $\alpha^{\text{Hep}}$  mice with PI3K $\alpha^{\text{F/F}}$  mice and only littermates from the same parents were used for the experiments. Mice were maintained at the EBM specific pathogen free facility of the University of Gothenburg under a 12-hour light / 12-hour dark cycles and at a room temperature of 22°C. For the *in vivo* studies littermate PI3K $\alpha^{\text{Hep}}$  mice and PI3K $\alpha^{\text{F/F}}$  mice were selected post hoc from a larger group of mice to match their body weight. For insulin-tolerance test (ITT) mice were fasted for 4 hours, from 7:00 AM to 11:00 AM, and injected intraperitoneally with 0.5 I.U. of insulin per Kg of body weight. Blood was collected from the tail at the indicated post-injection times and blood glucose concentrations were measured using a glucometer. For glucose tolerance test (GTT) mice were fasted as described above for the insulin tolerance test, then were injected intraperitoneally with 2g of glucose per Kg of body weight. Blood was collected from the tail at the indicated time-points and used to measure blood glucose and prepare serum for insulin measurements. Serum insulin was measured using a commercially available ELISA kit (Crystal Chem). For the *in vivo* analysis of PI3K $\beta$  inhibition, 2 mg/kg of TGX221 or a control solution (without TGX221) were injected intraperitoneally into three-months-old PI3K $\alpha^{\text{Hep}}$  male mice or PI3K $\alpha^{\text{F/F}}$  littermate male mice. The injectable solutions were prepared under laminar flow as following: 1,6% TGX-221 (from a 32,92 mM stock in DMSO), 30% PEG, 1% Tween-80 in PBS; or control “vehicle solution” without TGX221 (1,6% DMSO, 30% PEG, 1% Tween-80 in PBS). Blood glucose and serum insulin were measured as for the GTT.

Mice for primary hepatocyte cell culture were as following: PI3K $\alpha^{\text{Hep}}$  and PI3K $\alpha^{\text{F/F}}$  control hepatocytes were from male mice in 129/SvJ and C57BL/6J mixed background as described above, whereas WT hepatocytes were from male mice in pure C57BL/6J genetic background.

Mice were anesthetized with Isoflurane (Baxter KDG 9623) and sacrificed by bleeding.

All mouse studies were approved by the Ethics Committee on Animal Care Use in Gothenburg, Sweden.

### Primary Hepatocyte Cell Cultures

For mouse primary hepatocyte preparations we used 12 to 18 week-old male mice, and littermate mice were used for experiments comparing hepatocytes from PI3K $\alpha^{\text{Hep}}$  mice with hepatocytes from PI3K $\alpha^{\text{F/F}}$  mice. Mice were anesthetized with Isoflurane (Baxter KDG 9623) and sacrificed by bleeding. Liver was perfused with 60 mL of washing solution consisting in 1x Hank's buffered salt solution (GIBCO 14170-112), without magnesium or calcium and with the addition of 0.5 mM EGTA, the liver was then perfused with a digestion medium: DMEM-low glucose (HyClone) with 1% Penicillin Streptomycin and 15mM HEPES and 0.8 mg/mL of collagenase type IV (SIGMA). The collagenase digestion was performed at 37°C for about 10 min, after which Glisson's capsule is teared apart using a pair of sterile forceps to release the collagenase-digested liver into a sterile 10 cm Petri dish containing 10 mL of medium under a cell culture hood. Hepatocytes are dispersed in the medium using a pipette and filtered through a 70  $\mu\text{M}$  cell strainer into a falcon tube. Cells are collected by centrifugation at room temperature at 50 g for 3 min and washed 3 times with 20 mL of 50% DMEM high-glucose 50% HAM'S F-12 with 10% FBS, 1% penicillin streptomycin and 100  $\mu\text{M}$  of dexamethasone. The cells were counted and viability was evaluated by trypan blue exclusion and plated in 12 well plates pre-coated the day before with type I collagen dissolved in 0.02N acetic acid. Hepatocytes were plated at a density of  $4 \cdot 10^5$  live cells per well in one ml of medium. From a 12-18 week old mouse 30-50 million hepatocytes were obtained with a viability of 80%–95% (typically  $\approx 90\%$ ) assessed by trypan blue exclusion.

Human primary hepatocytes from donors were from a commercial provider, BioreclamationIVT. The culture of primary human hepatocytes was established in our laboratory in collaboration with Astrazeneca (Dr. Maria Chiara Magnone Sr Director, Head of Translational Sciences IMED CVMD). BioreclamationIVT is an approved AstraZeneca provider complying with the company Human Biological Samples policies. The cells were thawed in 37°C pre-warmed InVitroGRO CP Medium (IVT) completed with Torpedo antibiotic mix (IVT, 1ml in 45 mL medium). Cells were counted and viability was evaluated by trypan blue exclusion and plated in 12 well plates pre-coated the day before with type I collagen dissolved in 0.02N acetic acid. Hepatocytes were plated at a density of  $4 \cdot 10^5$  live cells per well in one ml of medium. Essential characteristics of primary hepatocytes donors are listed in [Table S2](#).

### Production and Precise Titration of Recombinant Adenoviruses

The recipient virusmid (VmAdcDNA3), which is based on adenovirus serotype-5 with E1/E3 deletions, was provided by Luciano Pirola Unité 1060 INSERM CarMen Lyon France, and was previously described (Chaussade et al., 2003). Recombinant adenoviruses expressing the gene of interest were obtained by homologous recombination in BJ5183 *E. Coli* between the VmAdcDNA3 recipient virusmid linearized with *Swa*I with the pcDNA3 plasmid bearing the specific gene of interest linearized with *Xmn*I. Recombinant clones were confirmed by PCR as described (Chaussade et al., 2003). Adenovirus packaging was performed by calcium phosphate transfection of *Pac*I-linearized recombinant virusmids into HEK293 cells, the virus was amplified in HEK293, purified on a cesium chloride gradient followed by dialysis in PBS with 10% glycerol and stored at  $-80^\circ\text{C}$ .

The GFP-expressing adenovirus was provided by Dr. Luciano Pirola, INSERM 1060 CarMen Lyon.

The GFP-Cre adenovirus was from the Coral Vector Core Facility, University of Iowa Health Care, Caver College of Medicine.

The PI3K $\beta$ -expressing adenovirus was generated by subcloning PI3K $\beta$  from pBacPAK p110 $\beta$  WT, a gift from Julian Downward (Addgene plasmid # 55724) (Fritsch et al., 2013).

p110 $\beta$  DNA was amplified by PCR from pBacPAK p110 $\beta$  WT using the following sequences: CCTAAAGGTACCTATGCCTCCTGCTATGGCAGAC inserting a restriction site for KpnI in position 11 at 5' and AACTCTCGAGGGACCTGTAGTCTTTCCGTACTGTG inserting a restriction site for XhoI in position 5 at 3'. The amplified DNA was purified and digested with the two restriction enzymes and cloned into a digested pCDNA3.1 plasmid using T4 ligase (New England Biolabs). This cloning strategy inserted an HA-tag that was located at the C-Terminal of p110 $\beta$ . This pcDNA3.1-PI3K $\beta$  was used to generate the PI3K $\beta$  expressing adenovirus by homologous recombination with VmAdcDNA3 packaging and purification as described above.

The H-RAS17N expressing adenovirus was generated using a pcDNA3.1+ bearing the cDNA of human H-RAS17N with three HA tags at the N terminus from UMR cDNA Resource Center, University of Missouri-Rolla (GB Acc. NM\_005343). Homologous recombination with VmAdcDNA3, packaging, and purification of the adenovirus were performed as described above.

The R-RAS43N expressing adenovirus was generated using a pcDNA3.1+ bearing the cDNA of human R-RAS43N with three HA tags at the N terminus from UMR cDNA Resource Center, University of Missouri-Rolla (GB Acc. NM\_006270). Homologous recombination with VmAdcDNA3, packaging, and purification of the adenovirus were performed as described above.

To titer the recombinant adenoviruses we first determined the titer of the GFP-expressing adenovirus using the Reed-Muench method and positivity of infection was defined by the presence of green fluorescent cells. This precisely titrated GFP-expressing adenovirus is used as "meter" to determine the titer of the other recombinant adenoviruses. For all the adenovirus not expressing the GFP a first estimate of adenoviral titer is performed by measuring optical density at 260 nm of the viral preparation. This titer is used only as a rough estimate and a final precise titer is measured by infecting Hepa 1-6 cells in triplicate with 10, 25, 50, and 100 MOI of the recombinant adenovirus, which are calculated using the approximate titer above (by optical density at 260 nm) in parallel with Hepa 1-6 cells infected as above but using the precisely titrated GFP-expressing adenovirus. 24 hours post infection the cells were fixed and stained with anti HA antibodies for immunofluorescence analysis of the efficiency of infection expressed as percentage of fluorescent cells on total cells. The final viral titer was thus calculated by direct comparison of the efficiency of infection in Hepa 1-6 cells using the GFP-expressing adenovirus (our control adenovirus) with the efficiency of infection observed in Hepa 1-6 cells using the virus expressing the HA-tagged transgene.

### Cell Culture Treatments and TUNEL Assay

The primary hepatocytes, mouse and human, were prepared as described above.

The pharmacological mapping of insulin induced-PI3K activity in mouse hepatocytes was performed by pre-incubation of hepatocyte cell cultures 30 min before insulin stimulation with culture medium containing the indicated doses of a specific isoform-selective PI3K inhibitor. After the 30 min pre-incubation period, hepatocytes were stimulated with 10 nM of insulin by adding insulin to the cell culture medium containing the specific PI3K inhibitor, after 8 min of insulin stimulation at 37°C, cells were washed once with ice-cold PBS and lysed with an ice-cold NP40-based lysis buffer containing phosphatases and proteases inhibitors. Cell lysates were immediately analyzed by immunoblot.

For experiments where hepatocytes are infected with recombinant adenoviruses the cells were plated in twelve well plates as described above and infected with the indicated multiplicity of infection (MOI), calculated as plaque forming units (PFU) per cell, twenty hours after plating the cells. Two hours after infection the medium was replaced with a new one without virus but containing serum, and twelve hours after infection the cells were placed for another twelve-hours period in a serum-free culture medium before insulin stimulation for eight minutes at the indicated dose or with 10 nM insulin at the indicated time. After insulin stimulation hepatocytes were lysed as indicated above for the pharmacological mapping. To evaluate adenovirus-induced toxicity the hepatocytes were treated as for the immunoblot analysis above, fixed with a cold (-20°C) 70% methanol 30% acetone solution and apoptosis was evaluated by TUNEL staining using a commercially available kit (TUNEL-Red Roche).

### PI3K $\beta$ Silencing in Primary Mouse Hepatocytes

Mouse primary hepatocytes were transfected with PI3K $\beta$ -specific siRNA (Dharmacon, ON-TARGET plus SMARTpool L-04088-00-0005) or a control siRNA (Dharmacon, ON-TARGET plus Control Pool Non-Targeting pool D-001810-10-05) for 48h using lipofectamine (ThermoFisher L3000150). siRNA was used at a final concentration of 25 nM in serum-free medium transfected with 1,87  $\mu$ L lipofectamine/well (12-well plate). The two solutions were mixed in a ratio 1:1, and incubated at room temperature for 15 min. The mix was then added to the cells dropwise and incubated at 37°C for 48 hours. The medium was changed every 24 hours.

### qPCR Analysis of Glucose-6-Phosphatase Gene Expression

Total RNA was obtained from primary hepatocytes by guanidinium-thiocyanate extraction method. cDNA was prepared using a reverse transcription kit (Promega, A3802), and qPCR was performed using a commercial SYBR green mix (Bio-Rad 172-5274) with glucose-6-phosphatase (G6P) specific primers and cyclophilin specific primers for normalization.

### Immunoblot Analysis

Protein samples were resolved by SDS-PAGE electrophoresis and transferred to a PVDF membrane. The membrane blocking was performed at room temperature in 3% bovine serum albumin (BSA), 0.3% tween solution in phosphate saline buffer (PBS).

Incubation with primary antibody was performed overnight in cold room in PBS with 0.3% tween and 3% BSA, the membranes were washed three times with a PBS 0.3% tween solution and incubated with an horseradish peroxidase conjugated secondary antibody (GE Healthcare) in PBS 0.3% tween 3% BSA for one hour at room temperature. After incubation with the secondary antibody membranes were washed three times with a PBS 0.3% tween solution incubated with detection reagent, signal acquisition was performed using the Biorad ChemiDoc apparatus and quantification of immunoblot signal was performed with the Biorad Image Lab software.

### Immunoprecipitations

Primary mouse hepatocytes were plated at a density of  $6 \times 10^6$  in a 10 cm Petri dish and infected with Adeno GFP or Adeno HRAS17N 100 MOI, or treated or not with TGX221 before insulin stimulation as described in the main text. The hepatocytes were washed once with PBS 1X and lysed with 0.7 mL of lysis Buffer (20 mM Tris-HCl pH 8, 5% v/v glycerol, 138 mM NaCl, 2.7 mM KCl, 1% Nonidet P-40, 1 mM DTT, 5 mM EDTA, 20  $\mu$ M leupeptin, 18  $\mu$ M pepstatin, 20 mM NaF, 1 mM sodium orthovanadate, 1 mM pNPP). The lysate was collected, proteins were quantified and 800-1000  $\mu$ g of protein extract were pre-incubated with 30  $\mu$ L of a 40% protein A/G Agarose (Santa Cruz, Protein A/G PLUS Agarose sc2003) in lysis buffer, for 30 min at 4°C on a rotating wheel, the supernatant was collected and the beads were discarded. The proteins were then incubated with 800 ng of primary antibody for 30 min at 4°C on a rotating wheel, then we added protein A/G Agarose in lysis buffer and incubated the samples for 3 hours at 4°C on a rotating wheel. The samples were centrifuged for 15 min at maximum speed at 4°C and washed 3 times with 0.5 mL of lysis buffer and twice with 0.5 mL of 0.1 M Tris-HCl pH 7.4, 0.5 M LiCl. The samples were then resuspended in SDS-PAGE sample buffer and analyzed by immunoblot using the indicated antibodies.

### PI3K Selective Inhibitors

The PI3K isoform-selective inhibitors AZD8835 and AZD8186 were provided by AstraZeneca (<https://openinnovation.astrazeneca.com/>), all the other PI3K isoform-selective inhibitors were purchased from Selleckchem. Inhibitors were dissolved in DMSO at a concentration of 10 mM freshly before treating the cells. The IC<sub>50</sub> values of the PI3K inhibitors above for PI3K $\alpha$ ; PI3K $\beta$ ; PI3K $\delta$ ; and PI3K $\gamma$  are listed in Table S1.

### QUANTIFICATION AND STATISTICAL ANALYSIS

Data are expressed as means, and error bars indicate standard errors. At least three biological replicates were used for each measurement, the exact number of biological replicates for a specific experiment is indicated in the figure legends. A “biological replicate” is a mouse for *in vivo* studies and for primary mouse hepatocyte studies, or a human donor for analysis using primary human hepatocytes. A single value for a biological replicate could be the average of values from technical replicates of the same biological replicate (e.g., different bands on the same blot from the same hepatocyte preparation from the same mouse are quantified and averaged to one number representing one biological replicate) but statistical comparisons were made only for averages of values from biological replicates. Concerning samples randomization and stratification, for human hepatocytes four commercial preparation from four random donors were used and the characteristics of the donors are shown in Table S2. For *in vivo* mouse studies weight-matched littermate mice were used and, when both sexes are investigated, males and females were analyzed separately. For primary hepatocyte cell cultures the effect of a treatment is measured for each biological replicate and expressed as relative to the same untreated biological replicate as control (e.g., an hepatocyte from human donors is treated with insulin in presence of H-RNA17 adenovirus and compared on the same gel to control-treated hepatocytes from the same donor). We did not perform blind analysis, but to minimize the risk of bias most experiments were replicated by two or three investigators to ensure reproducibility. Concerning sample size determination, the number of mice used for *in vivo* studies was based on our previous experience, for cell culture studies a minimum of 3 biological replicates was analyzed when samples are loaded on the same gel and parametric statistical tests is used, whereas a minimum of 4 biological replicates was analyzed when non-parametric statistical tests were used. No data or biological replicate was excluded except from the *in vivo* data where mice were selected to be weight-matched. In analysis where two different categorical variables are considered (GTT, ITT, mice weight gain, and time-course analyses), two-way ANOVA was used. Immunoblot analysis of dose response treatments was performed by linear regression. Mann-Whitney test was applied for statistical analysis of single comparison of unpaired group samples loaded on different gels. t test analysis was used for TUNEL assay and to compare immunoblot data where all samples are loaded within the same gel. All statistical analysis was performed with GraphPad Prism software.